

Experimental and Theoretical Study of the Reactions between Neutral Vanadium Oxide Clusters and Ethane, Ethylene, and Acetylene

Feng Dong,[†] Scott Heinbuch,[‡] Yan Xie,[†] Jorge J. Rocca,[‡] Elliot R. Bernstein,^{*,†}
Zhe-Chen Wang,[§] Ke Deng,^{||} and Sheng-Gui He^{*,§}

Department of Chemistry, Department of Electrical and Computer Engineering, NSF ERC for Extreme Ultraviolet Science and Technology, Colorado State University, Fort Collins, Colorado 80523, Beijing National Laboratory for Molecular Science, State Key Laboratory for Structural Chemistry of Unstable and Stable Species, Institute of Chemistry, Chinese Academy of Sciences, Zhongguancun, Haidian, Beijing 100080, China, and National Center of Nanoscience and Technology, Beijing 100080, People's Republic of China

Received August 14, 2007; E-mail: erb@lamar.colostate.edu; shengguihe@iccas.ac.cn

Abstract: Reactions of neutral vanadium oxide clusters with small hydrocarbons, namely C₂H₆, C₂H₄, and C₂H₂, are investigated by experiment and density functional theory (DFT) calculations. Single photon ionization through extreme ultraviolet (EUV, 46.9 nm, 26.5 eV) and vacuum ultraviolet (VUV, 118 nm, 10.5 eV) lasers is used to detect neutral cluster distributions and reaction products. The most stable vanadium oxide clusters VO₂, V₂O₅, V₃O₇, V₄O₁₀, etc. tend to associate with C₂H₄ generating products V_mO_nC₂H₄. Oxygen-rich clusters VO₃(V₂O₅)_{n=0,1,2,...}, (e.g., VO₃, V₃O₈, and V₅O₁₃) react with C₂H₄ molecules to cause a cleavage of the C=C bond of C₂H₄ to produce (V₂O₅)_nVO₂CH₂ clusters. For the reactions of vanadium oxide clusters (V_mO_n) with C₂H₂ molecules, V_mO_nC₂H₂ are assigned as the major products of the association reactions. Additionally, a dehydration reaction for VO₃ + C₂H₂ to produce VO₂C₂ is also identified. C₂H₆ molecules are quite stable toward reaction with neutral vanadium oxide clusters. Density functional theory calculations are employed to investigate association reactions for V₂O₅ + C₂H_x. The observed relative reactivity of C₂ hydrocarbons toward neutral vanadium oxide clusters is well interpreted by using the DFT calculated binding energies. DFT calculations of the pathways for VO₃+C₂H₄ and VO₃+C₂H₂ reaction systems indicate that the reactions VO₃+C₂H₄ → VO₂CH₂ + H₂CO and VO₃+C₂H₂ → VO₂C₂ + H₂O are thermodynamically favorable and overall barrierless at room temperature, in good agreement with the experimental observations.

Introduction

Transition metal oxide materials have been widely applied in the petroleum, chemical, and environmental industries as heterogeneous catalysts and catalytic supports.^{1–7} Vanadium oxides are important transition metal oxide catalysts, both by themselves and deposited on the surface of other oxide supports.^{8,9} Vanadium oxide based catalysts are used in the

manufacture of important chemicals; for example, in the oxidation of SO₂ to SO₃ in the production of sulfuric acid,¹⁰ in selective oxidation of hydrocarbons, and partial oxidation of methane to formaldehyde, etc.¹¹ A detailed understanding of heterogeneous catalysis at an atomic, mechanistic, and electronic state level is still not available; however, gas-phase studies of transition metal oxide cluster reactions can provide insight into the mechanism of elementary reactions in catalytic processes at an atomic and molecular level.^{12–15} Gas-phase clusters are considered to be an ideal model system for local active sites of condensed/surface phases because they have relatively well-

[†] Department of Chemistry and NSF ERC for Extreme Ultraviolet Science and Technology, Colorado State University.

[‡] Department of Electrical and Computer Engineering and NSF ERC for Extreme Ultraviolet Science and Technology, Colorado State University.

[§] Beijing National Laboratory for Molecular Science, State Key Laboratory for Structural Chemistry of Unstable and Stable Species, Institute of Chemistry, Chinese Academy of Sciences.

^{||}National Center of Nanoscience and Technology.

- (1) (a) Fierro, J. L. G. *Metal Oxides Chemistry and Applications*, Taylor & Francis: London, 2006. (b) Thomas, C. L. *Catalytic Processes and Proven Catalysts*; Academic Press: New York, 1970.
- (2) Cornils, B.; Herrmann, W. A. *Applied Homogeneous Catalysis with Organometallic Compounds*, VCH: Weinheim, 1996; Vol. 51. 1, 2.
- (3) Bell, A. T. *Science* **2003**, 299, 1688.
- (4) Schroder, D.; Schwarz, H. *Angew. Chem., Int. Ed. Engl.* **1995**, 34, 1973.
- (5) O'Hair, R. A. J.; Vrkic, A. K.; James, P. F. *J. Am. Chem. Soc.* **2004**, 126, 12173.
- (6) Waters, T.; O'Hair, R. A. J.; Wedd, A. G. *J. Am. Chem. Soc.* **2003**, 125, 3384.
- (7) Barteau, M. A. *Chem. Rev.* **1996**, 96, 1413.

- (8) Weckhuysen, B. M.; Keller, D. E. *Catal. Today* **2003**, 78, 25.
- (9) Martinez-Huerta, M. V.; Gao, X.; Tian, H.; Wachs, I. E.; Fierro, J. L. G.; Banares, M. A. *Catal. Today*, **2006**, 118, 279–287.
- (10) Dunn, J. P.; Stenger, H. G.; Wachs, I. E. *Catal. Today* **1999**, 51, 301.
- (11) (a) Ertl, G.; Knozinger, H.; Weitkamp, J. *Handbook of Heterogeneous Catalysis*; Wiley-VCH: Weinheim, 1997. (b) Banares, M. A.; Alemany, L. J.; Granados, M. L.; Faraldos, M.; Fierro, Catal, J. L. G. *Today* **1997**, 33, 73. (c) Herman, R. G.; Sun, Q.; Shi, C.; Klier, K.; Wang, C. B.; Hu, H. C.; Wachs, I. E.; Bhasin, Catal, M. M. *Today* **1997**, 37, 1.
- (12) Ogliaro, F.; Harris, N.; Cohen, S.; Filatov, M.; de Visser, S. P.; Shaik, S. *J. Am. Chem. Soc.* **2000**, 122, 8977.
- (13) Muetterties, E. L. *Science* **1977**, 196, 839.
- (14) Bohme, D. K.; Schwarz, H. *Angew. Chem. Int. Ed.* **2005**, 44, 2336.
- (15) Zemski, K. A.; Justes, D. R.; Bell, R. C.; Castleman, A. W., Jr., *J. Phys. Chem. A* **2001**, 105, 4410.

defined structures, size-dependent properties, and are readily accessible by theory.^{16–18} Alternatively, a full understanding of the catalytic behavior of gas-phase clusters can, in principle, provide insight into the mechanism of practical catalyst systems and their design and synthesis.

The reactions of transition metal oxides in particular with hydrocarbons are of interest because of their importance in catalytic processes. These reactions involve C–H and C–C bond activation followed by elimination of hydrogen and small alkane groups.^{19–21} The cleavage of C–C bonds by heterogeneous catalysts is a key step in the process of larger hydrocarbons cracking into smaller molecules for the generation of petroleum based products. Vanadium oxides are one of the most important catalysts used in these industrial catalytic processes. To explore the detailed mechanism of these reactions at an atomic and molecular level, the reactivity of vanadium oxide cluster ions with small hydrocarbon compounds has been studied in the gas phase using mass spectrometric techniques^{22–32} in conjunction with theoretical studies.^{33–40} The reaction of mass-selected $V_4O_{10}^+$ with CH_4 has been studied by Feyel and co-workers²⁴ using a quadrupole-based mass spectrometer coupled with an electrospray ionization (ESI) source. They identify a C–H bond activation reaction, $V_4O_{10}^+ + CH_4 \rightarrow V_3O_9OH^+ + CH_3$, employing experiments and theoretical calculations. They also studied the gas-phase oxidation of propane (C_3H_8) and 1-butene (C_4H_8) by the $V_3O_7^+$ cluster ion. Oxidative dehydrogenation (ODH) of hydrocarbons by $V_3O_7^+$ is identified as a major reaction channel, while a minor channel involving C–C

bond cleavage to produce $V_3O_7(C_2H_4)^+$ is also observed.⁴¹ The reactions of mass selected $V_mO_n^+$ with ethane (C_2H_6) and ethylene (C_2H_4) were investigated by guided ion beam mass spectroscopy coupled with a laser ablation source.^{25,28,33} The major reaction channels observed in these experiments are associations and oxygen transfers. Oxygen transfer reaction pathways are identified for $(V_2O_5)_n^+$ cations reacting with C_2H_4 and C_2H_6 molecules. Calculations provide evidence that oxygen transfer reaction pathways are the most energetically favorable for $V_2O_5^+$ and $V_4O_{10}^+$ reacting with C_2H_4 via a radical cation mechanism. The reactions of $V_mO_n^-$ anions with C_2H_4 and C_2H_6 are also investigated, but no reaction products are found.²⁵

Most efforts to elucidate the properties and behavior of metal oxide clusters deal with ionic systems because cluster ions can be made directly from an ablation source and selected through some sort of mass filter (e.g., time-of-flight, quadrupole, magnetic sector, etc.). Recently, mass selected infrared photo-dissociation spectroscopy is employed to investigate structure of V_mO_n cluster ions.²⁶ Ionic clusters represent a model of some suggested defect sites in solids. Partial charge transfer between metal oxide clusters and support materials (either bulk or surface) may play an important role in catalytic processes in the condensed phase. In order to elucidate in detail the molecular mechanism of reactions between vanadium oxide clusters and hydrocarbons, many theoretical studies have been carried out, but most of these studies also focus on cluster ion reactions related to experimental results.^{23–28,33–34,41–43} Nonetheless, cluster ions are clearly much more reactive than their condensed-phase analogues and neutral molecules because of their net charge.^{34,44,45}

Dobler et al.³⁴ studied the oxidation of methanol to formaldehyde on silica supported vanadium oxide by density functional theory (DFT). They conclude that the mechanism for the radical cation and the neutral molecule reaction is the same, but that the energy profile changes substantially. The enthalpy changes from endothermic for the neutral molecule to exothermic for radical cation, and the energy barrier is lowered by as much as 70 kJ/mol for the ionic reaction with respect to that of the neutral reaction. Thus, neutral clusters can supply useful information concerning true catalytic reaction sites on metals or metal oxide surfaces in bulk/condensed-phase systems. Neutral clusters are, however, more difficult to study because they cannot be size selected and one must find a valid method to ionize neutral species without fragmentation, especially for metal oxide clusters with high ionization energies (IE). For example, the IEs of vanadium oxide clusters are around 8–10 eV or even higher for oxygen rich clusters (e.g., VO_3 , V_3O_8 ,...).⁴⁶ Typical multiphoton and electron impact ionization techniques almost always cause severe cluster fragmentation, and thus loss of original neutral cluster information.

Recently, we have employed a new desktop, 26.5 eV/photon (46.9 nm), soft X-ray (extreme ultraviolet, EUV) laser to study

- (16) Schlogl, R.; Abd, Hamid, S. B. *Angew. Chem. Int. Ed.* **2004**, *43*, 1628.
- (17) de Bruin, B.; Budzelaar, P. H. M.; Gal, A. W. *Angew. Chem. Int. Ed.* **2004**, *43*, 4142.
- (18) Reuter, K.; Frenkel, D.; Scheffler, M. *Phys. Rev. Lett.* **2004**, *93*, 116105.
- (19) Van Koppen, P. A. M.; Brodbeltustig, J.; Bowers, M. T.; Dearden, D. V.; Beauchamp, J. L.; Fisher, E. R.; Armentrout, P. B. *J. Am. Chem. Soc.* **1991**, *113*, 2359.
- (20) Van Koppen, P. A. M.; Brodbelt-Lustig, J.; Bowers, M. T.; Dearden, D. V.; Beauchamp, J. L.; Fisher, E. R.; Armentrout, P. B. *J. Am. Chem. Soc.* **1990**, *112*, 5663.
- (21) Van Koppen, P. A. M.; Bowers, M. T.; Fisher, E. R.; Armentrout, P. B. *J. Am. Chem. Soc.* **1994**, *116*, 3780.
- (22) Zemski, K. A.; Justes, D. R.; Castleman, A. W., Jr. *J. Phys. Chem. B* **2002**, *106*, 6136.
- (23) Shyue, J. J.; De Guire, M. R. *J. Am. Chem. Soc.* **2005**, *127*, 12736.
- (24) Feyel, S.; Dobler, J.; Schroder, D.; Sauer, J.; Schwarz, H. *Angew. Chem. Int. Ed.* **2006**, *45*, 4681.
- (25) Zemski, K. A.; Justes, D. R.; Castleman, A. W., Jr. *J. Phys. Chem. A* **2001**, *105*, 10237.
- (26) (a) Asmis, K. R.; Brummer, M.; Kaposta, C.; Santambrogio, G.; von Helden, G.; Meijer, G.; Rademann, K.; Woste, L. *Phys. Chem. Chem. Phys.* **2002**, *4*, 1101. (b) Brummer, M.; Kaposta, C.; Santambrogio, G.; Asmis, K. R.; *J. Chem. Phys.* **2003**, *119*, 12700.
- (27) (a) Bell, R. C.; Castleman, A. W., Jr. *J. Phys. Chem. A* **2002**, *106*, 9893. (b) Zemski, K. A.; Bell, R. C.; Castleman, A. W., Jr. *J. Phys. Chem. A* **2000**, *104*, 5732.
- (28) Moore, N. A.; Mitric, R.; Justes, D. R.; Bonacic-Koutecky, V.; Castleman, A. W., Jr. *J. Phys. Chem. B* **2006**, *110*, 3015.
- (29) Feyel, S.; Schroder, D.; Schwarz, H. *J. Phys. Chem. A* **2006**, *110*, 2647.
- (30) Bell, R. C.; Zemski, K. A.; Castleman, A. W., Jr. *J. Cluster. Sci.* **1999**, *10*, 509.
- (31) Bell, R. C.; Zemski, K. A.; Kerns, K. P.; Deng, H. T.; Castleman, A. W., Jr. *J. Phys. Chem. A* **1998**, *102*, 1733.
- (32) Fielicke, A.; Rademann, K. *Phys. Chem. Chem. Phys.* **2001**, *4*, 2621.
- (33) Justes, D. R.; Mitric, R.; Moore, N. A.; Bonacic-Koutecky, V.; Castleman, A. W., Jr. *J. Am. Chem. Soc.* **2003**, *125*, 6289.
- (34) Dobler, J.; Pritzsche, M.; Sauer, J. *J. Am. Chem. Soc.* **2005**, *127*, 10861.
- (35) Fielicke, A.; Mitric, R.; Meijer, G.; Bonacic-Koutecky, V.; von Helden, G. *J. Am. Chem. Soc.* **2003**, *125*, 15716.
- (36) Cheng, M. J.; Chenoweth, K.; Oxgaard, J.; van Duin, A.; Goddard, W. A., III. *J. Phys. Chem. C* **2007**, *111*, 5115.
- (37) Broclawik, E.; Haber, J.; Piskorz, W. *Chem. Phys. Lett.* **2001**, *333*, 332.
- (38) Gracia, L.; Sambrano, J. R.; Safont, V. S.; Calatayud, M.; Beltran, A.; Andres, J. *J. Phys. Chem. A* **2003**, *107*, 3107.
- (39) Gracia, L.; Andres, J.; Safont, V. S.; Beltran, A. *Organometallics* **2004**, *23*, 730.
- (40) Gracia, L.; Sambrano, J. R.; Andres, J.; Beltran, A. *Organometallics* **2006**, *25*, 1643.

- (41) Feyel, S.; Schroder, D.; Rozanska, X.; Sauer, J.; Schwarz, H. *Angew. Chem., Int. Ed.* **2006**, *45*, 4677.
- (42) Gracia, L.; Andres, J.; Safont, V. S.; Beltran, A. *Organometallics*, **2004**, *23*, 730.
- (43) Gracia, L.; Sambrano, J. R.; Safont, V. S.; Calatayud, M.; Beltran, A.; Andres, J. *J. Phys. Chem. A* **2003**, *107*, 3017.
- (44) Futrell, J. H. *Gaseous Ion Chemistry and Mass Spectrometry*; Wiley: New York, 1986.
- (45) Eller, K.; Schwarz, H. *Chem. Rev.* **1991**, *91*, 1121.
- (46) Matsuda, Y.; Bernstein, E. R. *J. Phys. Chem. A* **2005**, *109*, 3803.

gas-phase cluster chemistry. Using this radiation, all of the species of neutral metal oxide clusters and the products that are generated from the reactions of metal oxide clusters and reactants can be detected. The soft X-ray laser not only ionizes all of the neutral clusters in these experiments, but it also is a very gentle ionization source that does not seriously fragment metal oxide clusters (e.g., vanadium, niobium, and tantalum oxide clusters) of interest⁴⁷ and even weakly bound $(\text{H}_2\text{O})_n$, $(\text{CH}_3\text{OH})_n$, $(\text{NH}_3)_n$, $(\text{SO}_2)_n$, and $(\text{CO}_2)_n$ van der Waals and hydrogen-bonded clusters.^{48–51} Recently, Ahmed et al. studied water clusters employing VUV photoionization (10–14 eV synchrotron radiation).⁵² They concluded that the water cluster distributions, obtained by 12 eV near threshold ionization in their experiments and by 26.5 eV ionization in our experiments, are almost the same. We consider that during the photoionization process, the photoelectron takes away most of the photon energy above ionization energy of the cluster, leaving only a small amount of excess energy in the cluster after ionization.

In studies of neutral V_mO_n , Nb_mO_n , and Ta_mO_n clusters,⁴⁷ cluster distributions obtained by 26.5 eV soft X-ray ionization are much the same as those distributions obtained with near threshold ionization by a 118 nm laser, with the exception that some oxygen-rich clusters cannot be ionized by the 118 nm light. So, the 26.5 eV, soft X-ray laser is an ideal light source with which to study neutral metal oxide cluster reactions. With this ionization source, we can detect all neutral cluster species and their reaction products.

In the present work, neutral vanadium oxide clusters are reacted with the C_2 hydrocarbons, C_2H_6 , C_2H_4 , and C_2H_2 . Reactants and products in these reactions are investigated by single photon ionization at 26.5 eV (46.9 nm) and 10.5 eV (118 nm). The most stable vanadium oxide clusters VO_2 , V_2O_5 , V_3O_7 , and V_4O_{10} undergo association reactions with C_2H_4 to form products $\text{V}_m\text{O}_n\text{C}_2\text{H}_4$. Neutral oxygen-rich vanadium oxide clusters with an odd number of vanadium atoms VO_3 – $(\text{V}_2\text{O}_5)_n$ (e.g., VO_3 , V_3O_8 , and V_5O_{13}) can react with C_2H_4 molecules to cleave the C=C bond of C_2H_4 and to produce $(\text{V}_2\text{O}_5)_n\text{VO}_2\text{CH}_2$ products. For the reactions of V_mO_n (general) clusters with C_2H_2 molecules, the association complexes $\text{V}_m\text{O}_n\text{C}_2\text{H}_2$ are assigned as the major reaction products. Additionally, a dehydration reaction channel is identified for the reaction $\text{VO}_3 + \text{C}_2\text{H}_2 \rightarrow \text{VO}_2\text{C}_2 + \text{H}_2\text{O}$. C_2H_6 molecules are not very reactive with neutral vanadium oxide clusters. In order to interpret experimental observations, DFT calculations are performed to study C_2 hydrocarbon association with V_2O_5 and the pathways for the reactions $\text{VO}_3 + \text{C}_2\text{H}_4$ and $\text{VO}_3 + \text{C}_2\text{H}_2$. DFT calculated results for these reactions are in good agreement with experimental observations.

2. Experimental Procedures

Experiments performed for this study of neutral cluster reactions involve a time-of-flight mass spectrometer (TOF–MS) coupled with

single photon ionization of reactants and products by two different lasers: photon energies 26.5 and 10.5 eV. As the experimental apparatus has been described in detail elsewhere,^{46–57} only a general outline of the experimental scheme will be presented here. Briefly, the neutral vanadium oxide clusters are generated in a conventional laser vaporization/supersonic expansion cluster source by laser ablation of vanadium foil into a carrier gas of 0.5% O_2 and He at 80 psig. A 532-nm wavelength laser (second harmonic of a Nd/YAG laser, 1064 nm) is employed to ablate the vanadium metal at 10–20 mJ/pulse. The reactant gases, pure C_2H_6 , C_2H_4 , and C_2H_2 , or their mixtures with He, are pulsed into the reactor tube located at 20 mm downstream from the exit of the expansion channel. The generated vanadium oxide clusters react with reactant gases in the flow tube reactor. The design of our flow tube reactor is similar to the one adopted by Smalley et al.^{58a} This method is commonly used in the study of elementary reactions of neutral metal clusters.⁵⁸ In this design, a flow tube reactor (70 mm length, \varnothing 6 mm) is coupled directly to the cluster formation channel (40 mm length, \varnothing 1.8 mm). After the flow tube reactor, the ions created in the ablation source and flow tube reactor are removed by an electric field. The possibility of charge exchange between the ions and much more abundant neutral species can be neglected based on the study of Kaldor et al.^{58bc} Additionally, the reactions of V_mO_n^\pm cluster ions with C_2H_x have been widely studied by mass-selected techniques.^{25,28,33,41} The products observed in these ion experiments are different from those formed in our neutral cluster studies. This gives us confidence that the products observed in our experiments are generated from neutral vanadium oxide clusters reacted with C_2H_x . Neutral clusters and reaction products pass through a skimmer with a 4-mm aperture into the ionization region of a time-of-flight mass spectrometer (Wiley–McLauran design, R.M. Jordan Co.). The neutral species are ionized by either a 118 nm (ninth harmonic of a seeded Nd/YAG 1064 nm laser⁵⁴) or a 46.9 nm EUV laser.⁵⁹ Ion signals generated from laser ionization are detected by a microchannel plate (MCP). In the 118 nm experiments, a two-chambered system is used to ensure that the TOF–MS chamber pressure is low enough (10^{-5} Torr) for the MCP voltages and the TOF–MS mean free path for ions. In this case, the reactant gases are diluted in He (5% $\text{C}_2\text{H}_x/\text{He}$) and are pulsed into the reactor. The instantaneous reactant gas pressure in the reactor cell is about 20 Torr so that good cooling is achieved for the neutral metal oxide clusters generated in the ablation source. 26.5 eV experiments are carried out in a single chamber system. Pure reactant gases are used in these experiments. The instantaneous reactant gas mixture pressure in the reactor cell is about 1 Torr in this set up. Neutral cluster temperatures in 26.5 eV experiments are higher than those in the 118 nm experiments. As different experimental conditions and ionization cross sections exist for these different wavelength experiments, some small difference in the observation of reaction products are found for the 10.5 and 26.5 eV experiments.

The EUV laser (26.5 eV/photon energy) emits pulses of about 1 ns duration with an energy/pulse of 10 μJ at a repetition rate of up to 12 Hz. A pair of gold-coated toroidal and plane mirrors is placed in a Z-fold configuration just before the ionization region of the TOF–MS to provide alignment and focusing capabilities for the laser with respect

- (47) Dong, F.; Heinbuch, S.; Rocca, J. J.; Bernstein, E. R. *J. Chem. Phys.* **2006**, *125*, 164318.
 (48) Matsuda, Y.; Bernstein, E. R. *J. Phys. Chem. A* **2005**, *109*, 314.
 (49) Dong, F.; Heinbuch, S.; Rocca, J. J.; Bernstein, E. R. *J. Chem. Phys.* **2006**, *125*, 154317.
 (50) (a) Heinbuch, S.; Dong, F.; Rocca, J. J.; Bernstein, E. R. *J. Chem. Phys.* **2006**, *125*, 154316. (b) Heinbuch, S.; Dong, F.; Rocca, J. J.; Bernstein, E. R. *J. Chem. Phys.* **2007**, *126*, 244301.
 (51) Dong, F.; Heinbuch, S.; Rocca, J. J.; Bernstein, E. R. *J. Chem. Phys.* **2006**, *124*, 224319.
 (52) Belau, L.; Wilson, K.R.; Leone, S. R.; Ahmed, M. *J. Phys. Chem. A* **2007**, *111*, 10075.

- (53) Matsuda, Y.; Shin, D. N.; Bernstein, E. R. *J. Chem. Phys.* **2004**, *120*, 4142.
 (54) Shin, D. N.; Matsuda, Y.; Bernstein, E. R. *J. Chem. Phys.* **2004**, *120*, 4157.
 (55) Matsuda, Y.; Shin, D. N.; Bernstein, E. R. *J. Chem. Phys.* **2004**, *120*, 4165.
 (56) He, S.-G.; Xie, Y.; Dong, F.; Heinbuch, S.; Jakubikova, E.; Rocca, J. J.; Bernstein, E. R. *J. Phys. Chem. A*, submitted.
 (57) He, S.-G.; Xie, Y.; Guo, Y. Q.; Bernstein, E. R. *J. Chem. Phys.* **2007**, *126*, 194315.
 (58) (a) Geusic, M. E.; Morse, M. D.; O'Brien, S. C.; Smalley, R. E. *Rev. Sci. Instrum.* **1985**, *56*, 2123. (b) Zakin, M. R.; Brickman, R. O.; Cox, D. M.; Kaldor, A. *J. Chem. Phys.* **1988**, *86*, 3555. (c) Zakin, M. R.; Brickman, R. O.; Cox, D. M.; Kaldor, A. *J. Chem. Phys.* **1988**, *88*, 6605. (d) Morse, M. D.; Geusic, M. E.; Heath, J. R.; Smalley, R. E. *J. Chem. Phys.* **1985**, *83*, 2293. (e) Knickelbein, M. B. *Annu. Rev. Phys. Chem.* **1999**, *50*, 79.
 (59) (a) Heinbuch, S.; Grisham, M.; Martz, D.; Rocca, J. J. *Opt. Express* **2005**, *13*, 4050. (b) Rocca, J. J.; Shlyaptev, V. N.; Tomasel, F. G.; Cortazar, O. D.; Hartshorn, D.; Chilla, J. L. A. *Phys. Rev. Lett.* **1994**, *73*, 2192. (c) Rocca, J. J. *Rev. Sci. Instrum.* **1999**, *70*, 3799.

to the molecular beam at the ionization region. Transmissivity of this Z-fold mirror system is about 60%. EUV laser light is not tightly focused in the ionization region to avoid multiphoton ionization and a space charge Coulomb effect due to He^+ ions. A large number of He^+ ions, produced by 26.5 eV ionization of He in the molecular beam, can broaden the mass spectral features. Since a 26.5 eV photon from the EUV laser is able to ionize the He carrier gas employed in the expansion, the MCP ion detector voltage is gated to reduce the MCP gain when He^+ arrives at the mass detector, in order to prevent detector circuit overload and saturation.

The 118 nm laser light is generated by focusing the third harmonic (355 nm, ~ 30 mJ/pulse) of a Nd:YAG laser in a tripling cell that contains about a 250 Torr argon/xenon (10/1) gas mixture. To separate the generated 118 nm laser beam from the 355 nm fundamental beam, a magnesium fluoride prism (apex angle = 6°), which was not employed in our previous studies,^{53–55} is inserted into the laser beams. In this case, one is quite sure that the mass signals are generated by ionization purely through the VUV laser radiation at low power (~ 1 μJ /pulse, pulse duration ~ 5 ns).

3. Computational Methods

DFT calculations are carried out using the Gaussian 03 program.⁶⁰ The B3LYP functional^{61–63} and TZVP basis set⁶⁴ are used. B3LYP/TZVP level of theory with moderate computational cost was tested to give reasonably good results for bond strengths of vanadium oxides.³³ The enthalpies of formation for C_2 hydrocarbons are also very well calculated at this level of theory. Binding energies between neutral V_2O_5 and C_2 hydrocarbons are calculated at different typical association geometries. This involves geometry optimizations and vibrational frequency calculations for V_2O_5 , C_2 hydrocarbons, and their association products. Extended calculations are performed to find possible (thermodynamically allowed) reaction channels and pathways for two reaction systems, $\text{VO}_3 + \text{C}_2\text{H}_4$ and $\text{VO}_3 + \text{C}_2\text{H}_2$. For each reaction channel, the calculation involves geometry optimization of various reaction intermediates and transition states through which the intermediates transfer to one another. Transition state optimizations are performed by using the Berny algorithm⁶⁵ or the synchronous transit-guided quasi-Newton (STQN) method.^{66,67} Vibrational frequency calculations are performed to check that reaction intermediates and transition state species have zero and one imaginary frequencies, respectively. Intrinsic reaction coordinate (IRC) calculations^{68,69} are also performed so that a transition state connects two appropriate local minima in the reaction pathways. The relaxed potential energy surface (PES) scan implemented in Gaussian 03 is extensively used to get good initial structures for the stable and transition states determined. In this method, once a stable

state is found, several relaxed PESs can be scanned for possible internal reaction coordinates. The maximum and new minimum in a relaxed PES correspond to good guesses for transition and new stable states, respectively. A complete reaction pathway will be eventually determined following this method. Binding energies are calculated for a few species employing the Basic Set Superposition Error (BSSE) correction;⁷⁰ these are found to be insignificant at the present level of theory.

4. Experimental Results

4.1. Reactions of V_mO_n Clusters with C_2H_x by 26.5 eV Ionization. In our previous studies,⁴⁷ vanadium oxide clusters (V_mO_n) are classified into three categories. The first category is the most stable neutral clusters for each V_m family, such as VO_2 , $\text{V}_2\text{O}_4/\text{V}_2\text{O}_5$, V_3O_7 , V_4V_{10} , V_5O_{12} , V_6O_{15} , etc. They dominate the cluster distribution in the mass spectrum under saturated oxygen concentration conditions (5% O_2/He expansion), and they have stable structures as demonstrated experimentally and theoretically.^{47,71,72} The second category is oxygen-rich clusters that have one more oxygen atom compared to the most stable clusters, such as VO_3 , V_2O_6 , V_3O_8 , V_5O_{13} , etc. These clusters present a higher tendency to lose O or O_2 and become the most stable clusters.⁷² The third category is oxygen-deficient clusters that have one or more oxygen atoms fewer than the most stable clusters, such as V_2O_3 , $\text{V}_3\text{O}_{5,6}$, and $\text{V}_4\text{O}_{8,9}$. These clusters present a higher tendency to react with O or O_2 and become the most stable clusters.⁷²

Figure 1a displays a TOF mass spectrum of V_mO_n clusters generated under a low oxygen concentration condition (0.5% O_2/He expansion) using a 26.5 eV soft X-ray laser for ionization. A number of oxygen-deficient clusters ($\text{V}_2\text{O}_{2,3}$, $\text{V}_3\text{O}_{5,6}$, V_4O_8 , etc.) are observed in the cluster distribution under this low O_2 concentration condition. Oxygen rich clusters (such as VO_3 , V_2O_6 , V_3O_8 , etc.) are also observed in the mass spectrum. Additionally, one can find some clusters with one or two hydrogen atoms, such as $\text{VO}_3\text{H}_{1,2}$, $\text{V}_2\text{O}_6\text{H}_{1,2}$ and $\text{V}_3\text{O}_8\text{H}_{1,2}$ etc. They are generated from oxygen rich clusters that react with trapped hydrogen in the metal or water in the system to produce $\text{V}_m\text{O}_n\text{H}_{1,2}$. Since the most stable oxidation states for vanadium are +4 and +5, VO_3 , V_2O_6 , and V_3O_8 etc, can readily form OH ligands to generate these preferred valence states. The same observations are also found for tantalum and niobium oxide clusters.⁴⁷ If vanadium oxide clusters are generated under oxygen saturation conditions (5% O_2/He expansion gas), then the population of the most stable clusters and oxygen-rich clusters will increase in the cluster distribution.⁴⁷ Apparently, such oxygen-rich clusters tend to be quite reactive.

To study neutral V_mO_n cluster reactions with hydrocarbons, the reactants, pure or diluted (in He), ethane (C_2H_6), ethylene (C_2H_4), and acetylene (C_2H_2) gases are individually and separately pulsed into the reactor. When the neutral clusters generated from the ablation/expansion source pass through the reactor cell, collisions will occur between neutral V_mO_n clusters and the hydrocarbons. A new distribution of neutral clusters and reaction products is obtained by using 26.5 eV laser ionization. As shown in Figure 1b, all of the cluster signals decrease in roughly the same proportion when C_2H_6 gas is added to the reactor cell. A similar result is also observed when inert

(60) Frisch, M. J.; Trucks, G. W.; Schlegel, H. B.; Scuseria, G. E.; Robb, M. A.; Cheeseman, J. R.; Montgomery, J. A., Jr.; Vreven, T.; Kudin, K. N.; Burant, J. C.; Millam, J. M.; Iyengar, S. S.; Tomasi, J.; Barone, V.; Mennucci, B.; Cossi, M.; Scalmani, G.; Rega, N.; Petersson, G. A.; Nakatsuji, H.; Hada, M.; Ehara, M.; Toyota, K.; Fukuda, R.; Hasegawa, J.; Ishida, M.; Nakajima, T.; Honda, Y.; Kitao, O.; Nakai, H.; Klene, M.; Li, X.; Knox, J. E.; Hratchian, H. P.; Cross, J. B.; Bakken, V.; Adamo, C.; Jaramillo, J.; Gomperts, R.; Stratmann, R. E.; Yazyev, O.; Austin, A. J.; Cammi, R.; Pomelli, C.; Ochterski, J. W.; Ayala, P. Y.; Morokuma, K.; Voth, G. A.; Salvador, P.; Dannenberg, J. J.; Zakrzewski, V. G.; Dapprich, S.; Daniels, A. D.; Strain, M. C.; Farkas, O.; Malick, D. K.; Rabuck, A. D.; Raghavachari, K.; Foresman, J. B.; Ortiz, J. V.; Cui, Q.; Baboul, A. G.; Clifford, S.; Cioslowski, J.; Stefanov, B. B.; Liu, G.; Liashenko, A.; Piskorz, P.; Komaromi, I.; Martin, R. L.; Fox, D. J.; Keith, T.; Al-Laham, M. A.; Peng, C. Y.; Nanayakkara, A.; Challacombe, M.; Gill, P. M. W.; Johnson, B.; Chen, W.; Wong, M. W.; Gonzalez, C.; Pople, J. A. *Gaussian 03*, revision C.02; Gaussian, Inc.: Wallingford, CT, 2004.

(61) Becke, A. D. *Phys. Rev. A* **1988**, *38*, 3098.
 (62) Becke, A. D. *J. Chem. Phys.* **1993**, *98*, 5648.
 (63) Lee, C. T.; Yang, W. T.; Parr, R. G. *Phys. Rev. B* **1988**, *37*, 785.
 (64) Schafer, A.; Huber, C.; Ahlrichs, R. *J. Chem. Phys.* **1994**, *100*, 5829.
 (65) Schlegel, H. B. *J. Comp. Chem.* **1982**, *3*, 214.
 (66) Peng, C. Y.; Schlegel, H. B. *Israel J. Chem.* **1994**, *33*, 449.
 (67) Peng, C. Y.; Ayala, P. Y.; Schlegel, H. B.; Frisch, M. J. *J. Comp. Chem.* **1996**, *17*, 49.
 (68) Gonzalez, C.; Schlegel, H. B. *J. Chem. Phys.* **1989**, *90*, 2154.
 (69) Gonzalez, C.; Schlegel, H. B. *J. Phys. Chem.* **1990**, *94*, 5523.

(70) (a) Boys, F.; Benardi, F. *Mol. Phys.* **1970**, *19*, 553. (b) Rappe, A. K.; Bernstein, E. R. *J. Phys. Chem. A* **2000**, *104*, 6117.

(71) Calatayud, M.; Andres, J.; Beltran, A. *J. Phys. Chem. A* **2001**, *105*, 9760.
 (72) (a) Jakubikova, E.; Rappe, A. K.; Bernstein, E. R. *J. Phys. Chem. A* accepted. (b) Jakubikova, E. Ph.D. Dissertation (May, 2007).

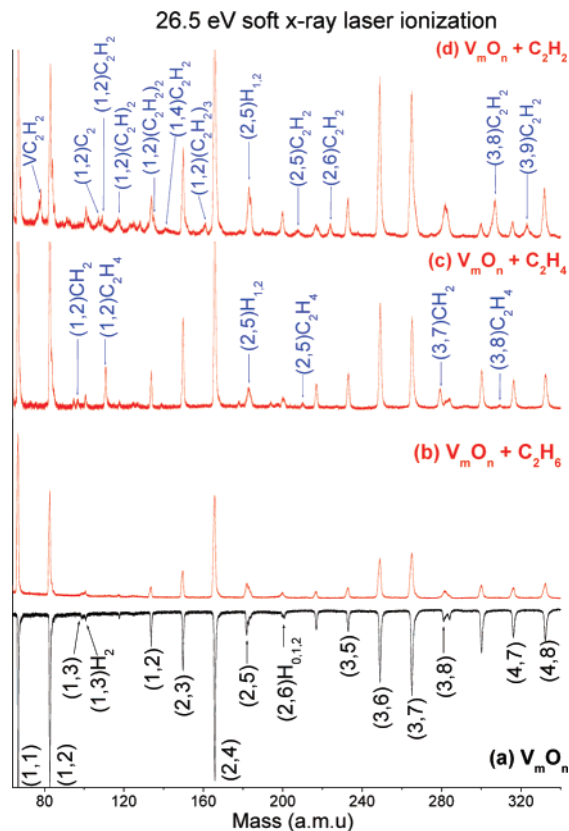


Figure 1. Reactions of V_mO_n clusters with C_2H_x studied by 26.5 eV soft X-ray laser ionization. New products of the reaction $V_mO_n + C_2H_x$ are detected. (a) V_mO_n cluster distribution generated with 0.5% O_2/He expansion gas. Reactant gases, (b) Pure C_2H_6 (c) Pure C_2H_4 . (d) Pure C_2H_2 , are added to the flow tube reactor, respectively.

gases are added to the reactor cell. Therefore, the decrease of cluster signals is due to scattering by the C_2H_6 gas pulsed into the reactor.

As shown in Figure 1c, the major products of the reaction $V_mO_n + C_2H_4$ are assigned as $VO_2C_2H_4$, $VO_3C_2H_4$, $V_2O_5C_2H_4$, and $V_3O_8C_2H_4$ generated from an association reaction channel,



The reaction products VO_2CH_2 and $V_3O_7CH_2$ are also observed in the mass spectrum. They must be produced from reactions that involve the cleavage of the $C=C$ bond of C_2H_4 . A close inspection of the mass regions around the clusters VO_3 , V_3O_8 , and V_5O_{13} (Figure 2) shows that VO_3 , V_3O_8 , and V_5O_{13} signals have disappeared when reactant C_2H_4 is added into flow tube reactor, this indicates that these oxygen rich clusters react with C_2H_4 . The possible reaction channels corresponding to the disappearance of VO_3 , V_3O_8 , and V_5O_{13} signals and the generation of VO_2CH_2 , $V_3O_7CH_2$ and $V_5O_{12}CH_2$ product signals will be discussed in the next section.

When C_2H_2 gas is added to the reactor, many new product signals, formed in the reaction of $V_mO_n + C_2H_2$, are observed in the mass spectra, as shown in Figure 1d. The major products, $VO_2C_2H_2$, $VO_3C_2H_2$, $V_2O_5C_2H_2$, $V_3O_8C_2H_2$, etc., are generated from the association reactions

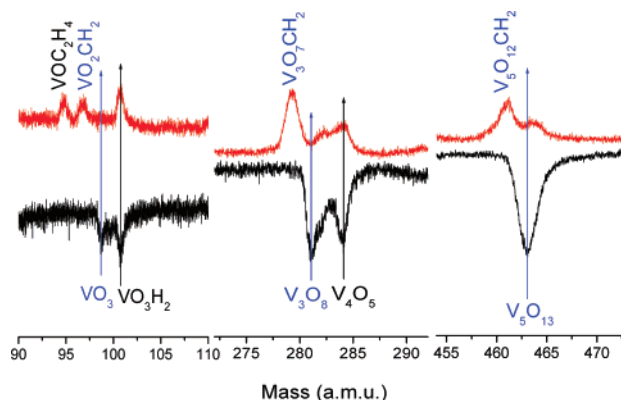


Figure 2. Reactions of V_mO_n clusters with C_2H_4 studied by 26.5 eV soft X-ray laser ionization. Expanded mass regions around oxygen rich clusters VO_3 , V_3O_8 , and V_5O_{13} . The lower spectra display V_mO_n cluster signals. The upper spectra display the signals of reaction products.

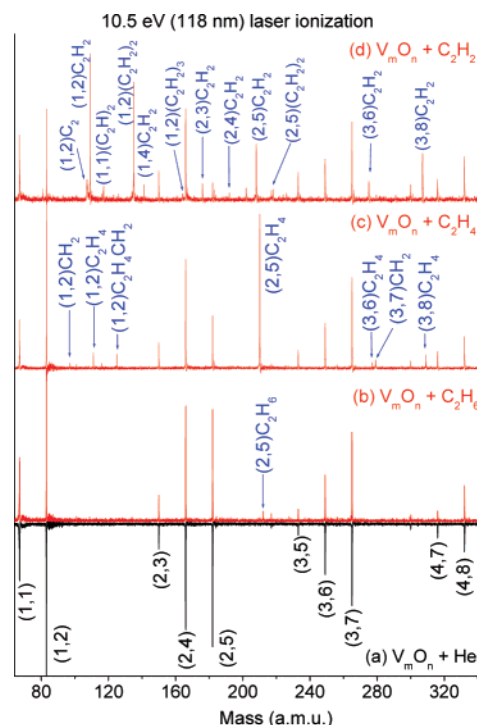


Figure 3. Reactions of V_mO_n clusters with C_2H_x studied by 118 nm (10.5 eV) laser ionization. (a) V_mO_n cluster distribution generated with a 0.5% O_2/He expansion gas, and added He gas in the flow tube reactor. Reactant gases, (b) Mixed 5% C_2H_6/He , (c) Mixed 5% C_2H_4/He , and (d) Mixed 5% C_2H_2/He , are added into flow tube reactor, respectively. The products detected by 10.5 eV laser are similar to those detected by 26.5 eV soft X-ray laser ionization.

Additionally, two new products, VO_2C_2 and $VO(C_2H)_2$, are found. These species may arise from dehydration reactions between VO_3 and C_2H_2 and VO_2 and $2C_2H_2$.

4.2. Comparison of 26.5 eV Ionization with 10.5 eV Ionization. The reaction of $V_mO_n + C_2H_x$ is also studied using the 118 nm laser ionization, as shown in Figure 3. In the 118 nm experiments, a two-chambered system is used, and in this case, the reactant gases are diluted in He (5% C_2H_x/He). In previous experiments, it has been proven that no fragmentation occurs during the ionization process since a single photon energy of 10.5 eV is not enough to fragment clusters after ionization. By comparison of Figure 1a with 3a, we find that the V_mO_n cluster distributions obtained by 26.5 and 10.5 eV ionizations

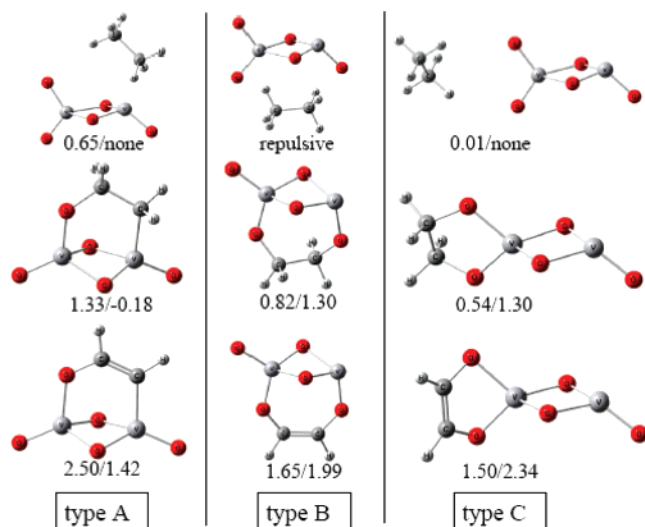


Figure 4. DFT optimized geometries of association products $V_2O_5C_2H_x$, $x = 6$ (top), 4 (middle), and 2 (bottom). Three types of geometry configurations (A, B, C) are presented. The values x_1/x_2 below each geometry are the zero-point vibrational energy corrected binding energies, in which x_1 and x_2 are the values for the association species in singlet and triplet spin states, respectively. For C_2H_6 , van der Waals association with V_2O_5 , the association species in triplet state corresponds to the V_2O_5 fragment in the triplet state. Triplet V_2O_5 is not populated in the experiment, so the binding energies are not determined for this case. See text for details.

are almost the same, except for the oxygen-rich clusters, VO_3 , V_2O_6 , V_3O_8 , etc., which are detected by 26.5 eV ionization (see Figure 2) but not by 10.5 eV ionization, because of the high ionization energy of these clusters.⁴⁷ Additionally, the $V_2O_4^+$ signal is much more intense than the $V_2O_5^+$ signal with 26.5 eV laser ionization. This result is contrary to the result obtained by 118 nm ionization, for which the $V_2O_5^+$ TOF-MS feature is much more intense than the $V_2O_4^+$ one. This behavior does not occur for Ta_2O_y and Nb_2O_y clusters; in those distributions, Nb_2O_5 and Ta_2O_5 are the predominant signal in the mass spectra using 26.5 eV ionization, and cluster distributions obtained by 26.5 and 10.5 eV ionization are almost the same.⁴⁷ The reason of this anomalous behavior is not clear but probably most readily associated with the specific details of wavelength-dependent ionization cross-sections for V_2O_4 and V_2O_5 neutral clusters.

Most of the reaction products observed in 10.5 eV ionization experiments are similar to those found by the 26.5 eV ionization experiments. Note that the products VO_2CH_2 and $V_3O_7CH_2$ generated from the reaction of $V_mO_n + C_2H_4$ are observed by both 10.5 and 26.5 eV ionization. It is found that some association products are only detected by 10.5 eV laser such as, $V_2O_5C_2H_6$, $V_2O_3C_2H_2$, $V_3O_6C_2H_2$, etc. We suggest that some relatively weak association products may be fragmented by 26.5 eV ionization while they might survive in the 118 nm experiment due to the near threshold ionization. Therefore, integrated information is provided by using both 10.5 and 26.5 eV ionization techniques. Additionally, the somewhat different experimental conditions for the 26.5 and 10.5 eV experiments may also contribute to slightly different observations for some association reaction products in the two experiments.

5. DFT Results

5.1 Association Products $V_2O_5C_2H_2$, $V_2O_5C_2H_4$, and $V_2O_5C_2H_6$.

Figure 4 presents the DFT optimized geometries

of association products $V_2O_5C_2H_x$ ($x = 2, 4, 6$) in three types (A, B, and C) of typical configurations. In the type A configuration, the two carbon atoms of C_2H_x connect with O and V atoms of V_2O_5 to form C–O and C–V bonds, respectively. In the type B configuration, the two carbon atoms connect with two oxygen atoms that are bonded to the two different V atoms of V_2O_5 . Two C–O bonds are formed in this type of product. In the type C configuration, two O–C bonds are formed, but both O atoms are connected to the same V atom. In the calculations, binding energies listed below each geometry are defined as $E(V_2O_5, \text{singlet}) + E(C_2H_x) - E(V_2O_5C_2H_x, \text{singlet/triplet})$. The V_2O_5 lowest triplet state is 0.71 eV higher in energy than its singlet ground state at this level of theory. The association species in singlet and triplet spin states are considered. The association reaction happens at near room temperature, so the binding energy is defined with V_2O_5 in the singlet state although the products may eventually be in the triplet state by a spin-inversion mechanism.⁷³ Two tendencies are found for these binding energies: 1. for each geometry type and each spin multiplicity, the binding energy increases as the hydrocarbon becomes more unsaturated; 2. for unsaturated hydrocarbons C_2H_4 and C_2H_2 , the binding energy of the singlet state decreases as the geometry type changes from A to B to C, while the binding energy of the triplet state increases. This behavior can be explained through the valance shell structure and oxidation state of vanadium atoms in these three types of configurations. In type A geometry, the two V atoms are in their most stable +5 state (terminal VO is a double bond), so the singlet state can be more stable than the triplet state when all valence electrons are bonded. In type B geometry, one V atom is in the +5 state and the other is in the +3 state. In type C geometry, both V atoms are in the +4 state. Therefore, in type B and type C configurations, the singlet state is less stable than the triplet state.

5.2 Reaction of VO_3 with C_2H_4 and C_2H_2 . DFT calculations are performed for VO_3 cluster reactions with C_2H_4 and C_2H_2 . The following reactions are calculated:



The values of the enthalpies of reactions (as given above) are obtained for the lowest energy structure of the reactants and products in their singlet or doublet spin states. These reactions are all thermodynamically allowed; however, they may not take place at room-temperature due to dynamic constraints. For example, barriers for the oxygen/hydrogen transfer and structure transformation, etc. may be quite high.

Figure 5 presents the DFT calculated relative Gibbs free energies at 298 K for various intermediates and transition states for reactions 3a and 3b, and the optimized geometries of

(73) Schroder, D.; Shaik, S.; Schwarz, H. *Acc. Chem. Res.* **2000**, *33*, 139.

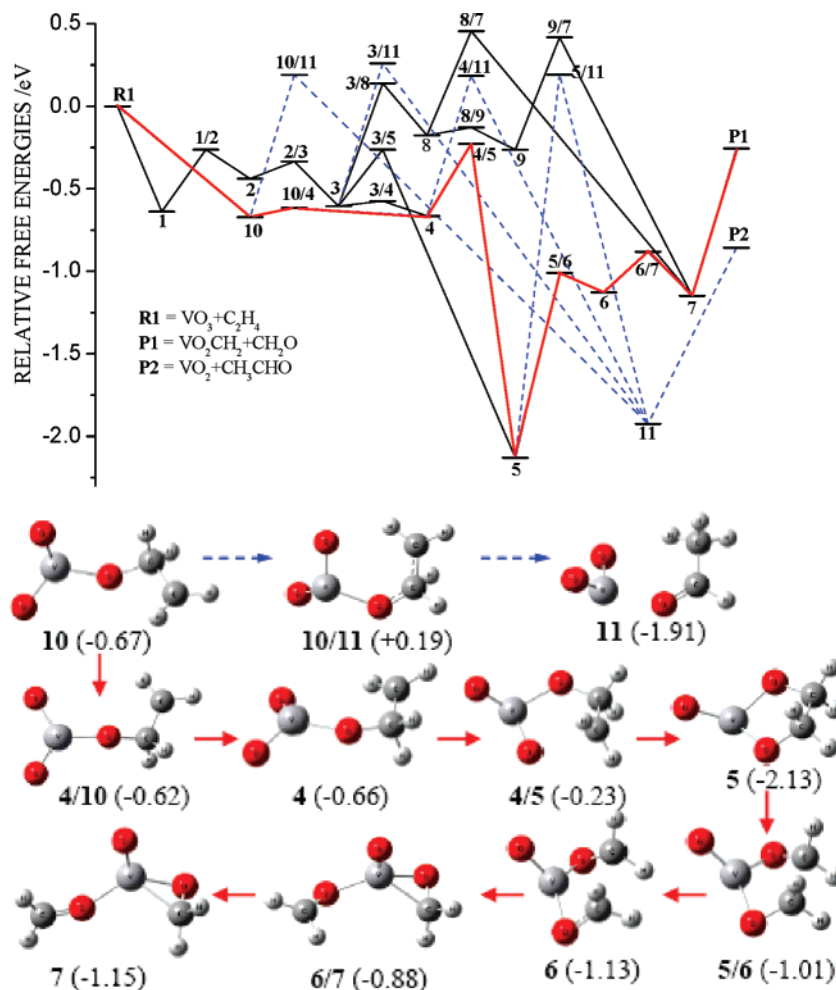
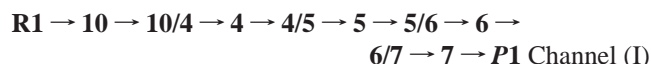


Figure 5. DFT calculated relative Gibbs free energies at 298 K for overall reactions $\text{VO}_3 + \text{C}_2\text{H}_4 \rightarrow \text{VO}_2\text{CH}_2 + \text{CH}_2\text{O}$ (**P1**) and $\text{VO}_3 + \text{C}_2\text{H}_4 \rightarrow \text{VO}_2 + \text{CH}_3\text{CHO}$ (**P2**). Structures are DFT optimized geometries of the reaction intermediates and the transition states in the lowest reaction pathway for generation of products **P1** and **P2**. The values (in eV) in parentheses below each geometry are Gibbs free energies at 298 K. DFT optimized geometries for all the reaction intermediates and the transition states can be found in Supporting Information.

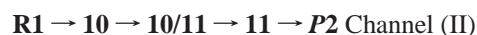
reaction intermediates and transition states for the lowest energy pathway:



C_2H_4 attacks an O atom of VO_3 to form intermediate **10**, and then transfer to **4** via transition state **10/4**. Surmounting a barrier to transition state **4/5**, a lowest energy intermediate **5** (−2.2 eV) with a five-membered ring, is formed. Through transition state **5/6**, the C–C bond of **5** ruptures and yields intermediate **6** ($\text{CH}_2\text{VO}_3\text{CH}_2$), in which two CH_2 radicals connect with two O atoms of VO_3 by C–O bonds. In intermediate **7**, the formation of a V–O–C three-membered ring weakens and stretches the V–O bond between the H_2CO moiety and the VO_2CH_2 moiety from 1.31 Å in **6** to 1.90 Å in **7**, and finally results in product **P1** ($\text{VO}_2\text{CH}_2 + \text{H}_2\text{CO}$). About 1 eV energy is required for breaking the V–O bond in this step. The large amount (>2 eV) of heat released from the formation of the most stable intermediate **5** is enough to overcome any barrier in the steps from intermediate **5** to product **P1**. The reaction channel (I) is a barrierless pathway for $\text{VO}_3 + \text{C}_2\text{H}_4 \rightarrow \text{VO}_2\text{CH}_2 + \text{CH}_2\text{O}$. Some reaction channels with high barriers (about 0.5 eV) are also found for reaction 3a as shown in Figure 5. These channels can be open under high-temperature conditions.

The DFT-determined structures presented in Figure 5 are comparable to those previously obtained for reactions of cationic vanadium oxide clusters (VO_2^+ , V_2O_5^+ , and $\text{V}_4\text{O}_{10}^+$) with C_2H_4 .^{33,38} Structures **10** and **4** have C_2H_4 moieties connected to terminal VO bonds through one C–O bond. Similar bonding patterns are found for reaction intermediates in the reaction $\text{V}_4\text{O}_{10}^+ + \text{C}_2\text{H}_4$. The important [3+2] cycloaddition structure **5** is also present in the reaction of V_2O_5^+ with C_2H_4 ; however, starting from this 3 + 2 intermediate, formaldehyde formation is more favorable than the acetaldehyde formation found in the reaction $\text{VO}_3 + \text{C}_2\text{H}_4$, while the opposite is true for the $\text{V}_2\text{O}_5^+ + \text{C}_2\text{H}_4$.³³ Structures (**1**, **2**, and **3**, see Supporting Information) with C_2H_4 moieties connected to the cluster with one or two V–C bonds are also determined as reaction intermediates in $\text{VO}_2^+ + \text{C}_2\text{H}_4$.³⁸

The formation of product $\text{CH}_3\text{CHO} + \text{VO}_2$ (**P2**, reaction 3b) is also thermodynamically favorable by 0.83 eV; however, obvious overall barriers exist in all reaction channels as shown in Figure 5. The lowest energy pathway is as follows:



All of the reaction channels involve a hydrogen transfer from one carbon to another carbon during the structure changes from

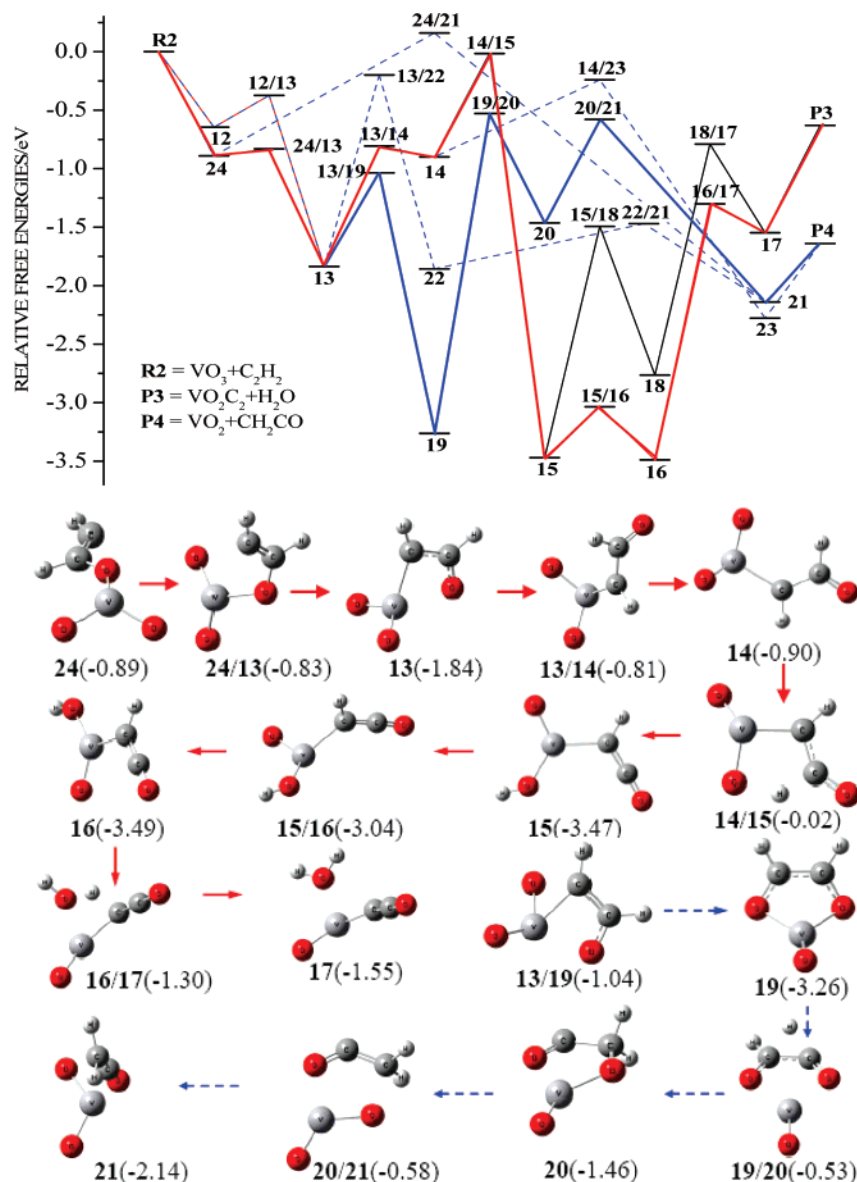
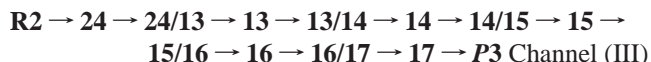


Figure 6. DFT calculated relative Gibbs free energies at 298 K for reaction channels $\text{VO}_3 + \text{C}_2\text{H}_2 \rightarrow \text{VO}_2\text{C}_2 + \text{H}_2\text{O}$ (**P3**) and $\text{VO}_3 + \text{C}_2\text{H}_2 \rightarrow \text{VO}_2 + \text{CH}_2\text{CO}$ (**P4**). The structures are the optimized geometries of the reaction intermediates and transition states of two lowest energy pathways for the generation of products **P3** and **P4**, respectively. The values (in eV) in parentheses below each geometry are Gibbs free energies at 298 K relative to reactants ($\text{R} = \text{VO}_3 + \text{C}_2\text{H}_2$). DFT optimized geometries for all the reaction intermediates and the transition states can be found in Supporting Information.

intermediates **3**, **4**, **5**, and **10** to **11**. The barrier heights of transition state **3/11**, **4/11**, **5/11**, and **10/11** are about 0.18~0.26 eV higher than the energy of reactant **R1**. Therefore, reaction 3b can occur as a high-temperature reaction, although the overall reaction is exothermic. We also calculate another possible pathway for a hydrogen transfer from carbon (intermediates **4**, **5**, and **10**) to oxygen to form vinyl alcohol as reaction 3c. It is also an exothermic reaction; however, the barriers are higher than the reactant **R1** energy. On the basis of the calculations, we conclude that the C–C bond breaking reaction (reaction 3a) is more favorable than reactions 3b and 3c, and channels (I) are the most favorable pathway for $\text{VO}_3 + \text{C}_2\text{H}_4$ reaction.

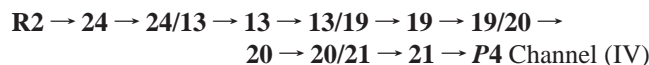
For reactions $\text{V}_m\text{O}_n + \text{C}_2\text{H}_2$, relative Gibbs free energies at 298 K for various intermediates, transition states, and their optimized geometries are obtained by DFT calculations as shown in Figure 6. The lowest energy reaction channel for the

generation of products **P3** is found (H_2O and VO_2C_2):



In the first step, C_2H_2 attacks an O atom of VO_3 to form intermediate **24**. As the C–V bond forms, one O atom migrates from VO_3 to C_2H_2 to yield **13** via transition state **12/13** or **24/13**. During this process, the C≡C bond of C_2H_2 is weakened to a C=C bond. After several steps, hydrogen atoms transfer from C atoms to the O atom as in channel (III), **13** transforms to intermediate **17**, in which H_2O attaches to VOC_2O by a binding energy of ~1 eV, and finally, H_2O leaves to generate product **P3** ($\text{H}_2\text{O} + \text{VO}_2\text{C}_2$).

The lowest energy reaction pathway for reactions $\text{V}_m\text{O}_n + \text{C}_2\text{H}_2$ to generate products **P4** (VO_2 and CH_2CO) is also a barrierless channel:



Intermediate **13** can also change structure to a five-membered ring structure of intermediate **19** (containing two C–O bonds). One V–O bond breaks to result in an O atom transfer from VO₃ to C₂H₂. The C–O bond cleavage of **20** yields **21**, which leads to final product **P4**. A barrier (0.167 eV) is found for oxygen abstraction channel **R2** → **24** → **24/21** → **21** → **P4**, in which oxygen atom directly transfers from VO₃ to C₂H₂.

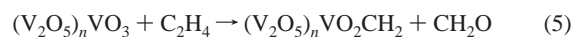
6. Discussion

6.1. Association Reactions of V_mO_n with C₂H₆, C₂H₄ and C₂H₂. Association reactions are found to be the main reaction channels for vanadium oxide clusters and C₂ hydrocarbons. As shown in Figure 3, with 118 nm ionization, V₂O₅C₂H₆ is the only product identified for the V_mO_n + C₂H₆ reaction. VO₂C₂H₄, V₂O₅C₂H₄, V₃O₆C₂H₄, and V₃O₈C₂H₄ are the association products identified for the V_mO_n + C₂H₄ reaction, and VO₂C₂H₂, V₂O₃C₂H₂, V₂O₄C₂H₂, V₂O₅C₂H₂, V₃O₈C₂H₂, etc. are the association products identified for the V_mO_n + C₂H₂ reaction. Unsaturated hydrocarbons C₂H₂ and C₂H₄ are more reactive with neutral vanadium oxide clusters than is the saturated hydrocarbon C₂H₆. Almost all V_mO_n clusters can form association products with C₂H₂, whereas most association products come from oxygen rich clusters and the most stable cluster of a given V_m family for the V_mO_n + C₂H₄ reaction. We conclude that C₂H₂ is more reactive than C₂H₄ for association reactions with V_mO_n.

As shown in Figure 3, the decay fractions ($I_0 - I$)/ I_0 (I_0 and I are the intensities of V₂O₅ signal before and after reaction with C₂H_x, respectively) of V₂O₅ signals in the reactions with C₂H₆, C₂H₄, C₂H₂ are 0.1, 0.6, and 0.86, respectively. With adopted experimental conditions such as estimated C₂H_x partial gas pressure (~1 Torr) and reaction time (~50 μs), we can provide an estimation of the first-order rate constants of three typical association reactions: $k(\text{V}_2\text{O}_5 + \text{C}_2\text{H}_6) = 7 \times 10^{-14} \text{ cm}^3 \text{ s}^{-1}$; $k(\text{V}_2\text{O}_5 + \text{C}_2\text{H}_4) = 6 \times 10^{-13} \text{ cm}^3 \text{ s}^{-1}$; and $k(\text{V}_2\text{O}_5 + \text{C}_2\text{H}_2) = 1 \times 10^{-12} \text{ cm}^3 \text{ s}^{-1}$. The observed reactivity tendency of C₂H_x in association reactions with neutral V₂O₅ is consistent with the calculated results. As shown in Figure 4, the saturated hydrocarbon C₂H₆ bonds weakly (0.65 eV) with V₂O₅, whereas C₂H₄ and C₂H₂ bond with V₂O₅ by CO and VC chemical bonds at 1.33 and 2.5 eV, respectively. On the basis of calculations, the association reactions of V₂O₅ + C₂H₄/C₂H₂ to generate V₂O₅C₂H₄ and V₂O₅C₂H₂ (type A, singlet) are barrierless processes at room temperature. According to the classical Rice–Ramsberger–Kassel–Markus (RRKM) theory: $k_{\text{dissociation}} = \nu (1 - E_{\text{bind}}/E)^{S-1}$, in which $E_{\text{activation}}$ is replaced by E_{bind} , the binding energy of (V₂O₅C₂H_x). A higher binding energy implies a slower dissociation rate constant and thus a longer lifetime for the meta-stable initial association intermediate (V₂O₅C₂H_x*). The V₂O₅C₂H_x* would eventually fall apart (V₂O₅ + C₂H_x) if no further reactions and/or collisions could remove excess energy in the association intermediate (V₂O₅C₂H_x*). In 118 nm flow tube experiments (mixture C₂H_x/He is added into flow tube), the longer lifetime of V₂O₅C₂H_x* means that the meta-stable species has more chance to be cooled by collisions, and thus a higher depletion rate of V₂O₅ cluster will be observed. Although Figure 3 addresses a specific cluster (V₂O₅) association with C₂ hydrocarbons, it reflects a general observation for all

V_mO_n clusters. This conclusion supports and is supported by the calculated results given in Figure 5 and 6 [compare VO₃C₂H₄ (**10**) with VO₃C₂H₂ (**24**), and VO₃C₂H₄ (**5**) with VO₃C₂H₂ (**19**)], as well as the experimental observations.

6.2. C=C Bond Breaking in (V₂O₅)_nVO₃ + C₂H₄ ($n = 0, 1, 2, \dots$) Reactions. New products VO₂CH₂, V₃O₇CH₂, and V₅O₁₂CH₂ are observed in the study of the V_mO_n + C₂H₄ reactions as shown in Figure 2. They can be produced from the following reactions:



in which $n = 0, 1, 2, \dots$. In reaction 5, oxygen-rich clusters VO₃–(V₂O₅) _{$n=0,1,2,\dots$} such as VO₃, V₃O₈, or V₅O₁₃, react with C₂H₄ and lose a CH₂O molecule. On the basis of DFT calculations, reaction 3a, VO₃ + C₂H₄ → VO₂CH₂ + CH₂O, is thermodynamically favorable by 0.25 eV, and is an overall barrierless reaction at a room temperature. Thus, VO₃ can be responsible for the generation of VO₂CH₂. One can then suggest that the general reaction 5 can occur and oxygen rich clusters VO₃–(V₂O₅) _{$n=0,1,2,\dots$} can cause C=C bond breaking for C₂H₄. In the TOF–MS (see Figure 2), oxygen-rich clusters VO₃, V₃O₈, and V₅O₁₃ disappear if C₂H₄ is added to the flow-tube reactor. H₂CO⁺ is not detected in these experiments with either 10.5 or 26.5 eV ionizations possibly because the ionization cross section for H₂CO (ionization energy 10.9 eV⁷⁴) is small at 26.5 eV, or because the concentration of the H₂CO product is too low to detect.

In reaction 6, the most stable clusters such as VO₂, V₃O₇, or V₅O₁₂, etc., react with C₂H₄, producing products VO₂CH₂, V₃O₇CH₂ or V₅O₁₂CH₂ and CH₂. We calculate ΔH_{298} for the reaction VO₂ + C₂H₄ → VO₂CH₂ + CH₂ based on following thermodynamic equations



ΔH_{298} for reaction 7 is obtained from our DFT calculation. Reaction 9 is not thermodynamically available at room temperature. Thus, VO₂CH₂ does not arise from reaction 9, and one can then deduce that C=C bond cleavage is not favorable for the most stable vanadium oxide clusters as given reaction 6.

VO₂CH₂, V₃O₇CH₂, and V₅O₁₂CH₂ products (see Figure 3) can also arise through fragmentation of association complexes, VO₂C₂H₄, V₃O₇C₂H₄, and V₅O₁₂C₂H₄, caused by 26.5 eV laser ionization. A 26.5 eV single photon energy is sufficient to break the C=C bond of V_mO_nC₂H₄, to produce V_mO_nCH₂ during the ionization process; however, VO₂CH₂ and V₃O₇CH₂ products are also observed in 10.5 eV ionization experiments (Figure 3). A single photon energy of 10.5 eV light is not high enough to rupture a C=C bond after ionization. Additionally, using the 26.5 eV laser, the photoionization products of the C₂H₄ molecule are measured as C₂H₄⁺ (30%), C₂H₃⁺ (35%), C₂H₂⁺ (28%), C₂H⁺ (3%), and CH₂⁺ (3%). We do not observe products like

(74) Tao, W.; Klemm, R. B.; Nesbitt, F. L.; Stief, L. J. *J. Phys. Chem.*, **1992**, *96*, 104.

$\text{VO}_2\text{C}_2\text{H}_3$ or $\text{V}_3\text{O}_7\text{C}_2\text{H}_3$ in the mass spectrum for the $\text{V}_m\text{O}_n + \text{C}_2\text{H}_4$ reaction, using 26.5 eV light for ionization. Moreover, association complexes $\text{VO}_2\text{C}_2\text{H}_4$, $\text{V}_2\text{O}_5\text{C}_2\text{H}_4$, and $\text{V}_3\text{O}_8\text{C}_2\text{H}_4$ are observed in the 26.5 eV ionization mass spectrum (see Figure 1). Thereby, VO_2CH_2 , $\text{V}_3\text{O}_7\text{CH}_2$, and $\text{V}_5\text{O}_{12}\text{CH}_2$ products are most probably generated from reaction 5, rather than from the fragmentation of $\text{VO}_2\text{C}_2\text{H}_4$, $\text{V}_3\text{O}_7\text{C}_2\text{H}_4$, and $\text{V}_5\text{O}_{12}\text{C}_2\text{H}_4$.

The C=C bond breaking and hydrocarbon selective oxidation occur only on oxygen rich neutral vanadium oxide clusters with composition $\text{VO}_3(\text{V}_2\text{O}_5)_n$. Examples from these studies are found for VO_3 , V_3O_8 , and V_5O_{13} , reacting with C_2H_4 . We also investigate the reactions of niobium and tantalum oxide clusters with C_2H_4 ; however, C=C bond breaking for C_2H_4 does not occur on any Nb_mO_n or Ta_mO_n clusters. For oxygen-deficient and stable V_mO_n clusters, only association reaction channels are identified. For vanadium oxide cluster cations reacting with C_2H_4 ,³³ the identified reaction channels are association and oxygen transfer. The reactions of V_mO_n^- anions with C_2H_4 have also been investigated, but no reaction products are found.³³

The cleavage of C=C bonds is a very important process for condensed phase catalysis. Formaldehyde is generated in reaction 5, and it is one of the most important fundamental industrial chemicals.¹¹ The mechanism of C=C bond breaking on VO_3 can be interpreted based on our DFT results shown in Figure 5 and 6. The first step of the process involves C–O bond formation, as well as C=C bond weakening to form intermediate **10**. The C=C double bond in $\text{CH}_2=\text{CH}_2$ (bond length = 0.1326 nm) is significantly weakened to become a single bond in intermediate **10** with C–C distances about 0.15 nm (C–C bond length = 0.1527 nm in C_2H_6). The second step in this development is the formation of a second C–O bond leading to the formation of a quite stable five-membered intermediate **5** (Figure 5), in which sufficient energy is released to break the C–C bond (**5** → **5/6** → **6**). The formation of intermediate **5** is a key step for C=C bond cleavage. For VO_3 , about 2.12 eV energy is released through intermediate **5** formation since the unstable oxidation states of VO_3 is stabilized by the formation of intermediate **5**: the oxidation state of V and O are (+4) and (–2), respectively, in this intermediate. Only 1.3 eV is released, however, as V_2O_5 forms the same five-membered ring association product as shown in Figure 4 (type C).

In the process of formaldehyde formation, acetaldehyde (CH_3CHO) formation is also possible. This latter reaction involves a hydrogen atom transfer from one carbon to another; however, the transfer barrier is high, as shown in Figure 5, so that acetaldehyde formation can only happen at high temperature. The reactions of cationic vanadium oxide clusters (V_mO_n^+) with ethylene have been studied by both experiments^{25,33,76} and DFT calculations.^{33,38} Formaldehyde formation does not occur on V_mO_n^+ clusters. In contrast, acetaldehyde formation is found over VO_2^{+76} and $(\text{V}_2\text{O}_5)_n^+$, $n = 1-3$,^{25,33} and this observation is supported by the DFT calculations.^{33,38} Hydrogen transfer barriers in these cationic species are around 0.13 eV – 1.45 eV depending on the reaction intermediates through which the transfer proceeds. In the neutral species studied in this work (Figure 5), hydrogen transfer barriers (0.84 – 2.32 eV) are

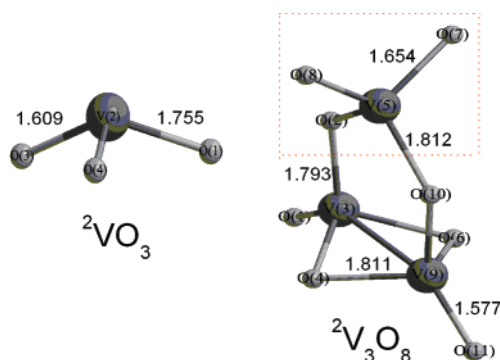


Figure 7. DTF calculated the lowest energy structures of VO_3 and V_3O_8 at B3LYP/TZVP level.

relatively high. Theoretical explanation of the C=C bond breaking process over V_mO_n^+ , not taken into account in the previous calculations,^{33,38–40} would be interesting to study.

These results for neutral vanadium oxide clusters suggest the question: why does C=C bond breaking only happen on oxygen rich vanadium oxide clusters with an odd number of vanadium atoms, $\text{VO}_3(\text{V}_2\text{O}_5)_n$? VO_3 has one more oxygen atom compared to the most stable vanadium oxide VO_2 ; therefore, it can be considered as an oxygen centered radical. DFT calculations show that VO_3 associates with C_2H_4 to form a stable five-membered ring intermediate **5**. A large amount of energy (2.12 eV) is then released, leading to C=C bond breaking (see Figure 5). A V_3O_8 structure (shown in Figure 7) can be generated from V_2O_5 bonded to VO_3 as a formula $(\text{V}_2\text{O}_5)(\text{VO}_3)$, in which V and O atoms of the V_2O_5 moiety are oxidation states +5 and –2, respectively. Thus, oxygen rich vanadium oxide clusters VO_3 , V_3O_8 , V_5O_{13} , etc. can be expressed by $\text{VO}_3(\text{V}_2\text{O}_5)_n$. These clusters have an oxygen centered radical (VO_3), which can exceed the barrier associated with formal [3+2] cycloaddition.

Oxygen-rich clusters containing an even number of V atoms ($\text{V}_2\text{O}_5)_n\text{O}$, such as V_2O_6 , V_4O_{11} , etc. are also a hypervalent species; however, cleavage of the C=C bond of C_2H_4 does not occur on these clusters. For oxygen-rich clusters $(\text{V}_2\text{O}_5)_n\text{O}$ reacting with C_2H_4 , oxygen transfer reactions forming the $\text{C}_2\text{H}_4\text{O}$ product may be more favorable than the formation of a stable five-membered ring structure, such as intermediate **5** (Figure 5). In addition, it is interesting to note that C=C bond breaking for C_2H_4 occurs on $\text{VO}_3(\text{V}_2\text{O}_5)_n$ clusters, but does not occur on Nb_mO_n and Ta_mO_n clusters. Cleavage of a C=C bond also does not occur for other clusters reaction with C_2H_4 : for example, Ti_mO_n , Co_mO_n , Si_mO_n , Fe_mO_n , etc. These results indicate that the activities of metal oxide clusters are dependent on many issues: bond energies, reaction barriers, reaction rates, etc., not only on the oxygen-rich or -poor nature of M_mO_n clusters.

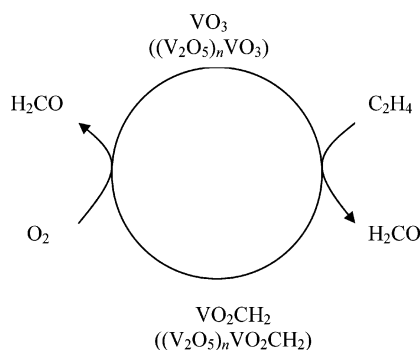
We suggest that the VO_3 moiety can be an active site for neutral vanadium oxide clusters. Evidence for an active moiety in gas-phase clusters further validates the idea that active sites of condensed phase oxide catalysts can be effectively modeled with gas-phase clusters. In practical catalysis, the selectivity of hydrocarbon partial oxidation is very important. In this work, we can present a catalytic model for formaldehyde formation through oxidation of C_2H_4 on VO_3 . Based on our calculations (B3LYP/TZVP), the reaction



(75) Chase, M.W., Jr. *NIST-JANAF Thermochemical Tables, Fourth Edition, J. Phys. Chem. Ref. Data, Monograph 9, 1998*, 1–1951.

(76) Harvey, J. N.; Diefenbach, M.; Schroder, D.; Schwarz, H. *Int. J. Mass Spectrom.* **1999**, *182*, 85.

Scheme 1



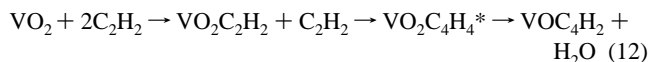
is thermodynamically available without a barrier. A catalytic cycle of C_2H_4 oxidation to H_2CO by VO_3 is suggested based on our experiments and theoretical calculations, as presented in Scheme 1.

Since VO_3 can thereby be employed in a catalytic cycle for C_2H_4 oxidation to H_2CO , other larger clusters of this general type ($VO_3(V_2O_5)_n$, $n=0,1,2,\dots$) can be active in a similar fashion. The understanding of the general characteristics of $VO_3(V_2O_5)_n$, $n=0,1,2,\dots$ would provide a possible opportunity for practical catalyst design for the synthesis of important chemicals (e.g., formaldehyde) through ethylene oxidation,



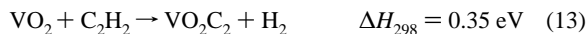
Further theoretical investigations on larger clusters are in progress.

6.3. Dehydration Reactions for $V_mO_n + C_2H_2$. Association reactions are the main channels for the reaction of $V_mO_n + C_2H_2$. Additionally, two new products, VO_2C_2 and VOC_4H_2 are observed in Figures 1d and 3d. VO_2C_2 can be produced from dehydration reactions 4a that are thermodynamically and dynamically favorable at room temperature (see Figure 6). VOC_4H_2 is suggested to be produced in the following reaction:



Shown in Figure 3d, the strong signals of intermediates $VO_2C_2H_2$ and $VO_2C_4H_4$ are observed, as well as an obvious depletion of the VO_2 signal, suggesting that the dehydration reactions 4a and 12 can occur under the present experimental conditions. On the basis of binding energy calculations shown in Figures 4 and 6, one can imagine that the vibrational temperature of intermediate $VO_2C_4H_4$ will be high if two acetylene molecules are bonded to VO_2 . Some of the intermediates $VO_2C_4H_4$ can be dehydrated to yield products $VOC_4H_2 + H_2O$ (reaction 12), and some can be collisionally cooled to form $VO_2C_2H_2$ and $VO_2C_4H_4$ as observed in mass spectra (Figures 1d and 3d).

Other possible reactions for the production of VO_2C_2 and VOC_4H_2 are the elimination of H_2 from $VO_2C_2H_2$ and $VO(C_2H_2)_2$, respectively, as follows:



DFT calculations show that ΔH_{298} for reaction 13 is endothermic by 0.35 eV, thus, this reaction will probably not occur under

present experimental conditions. No significant depletion of VO relative to VO_2 is observed when C_2H_2 is added to the reactor, and no new product signal for reaction intermediate VOC_2H_2 is detected in the mass spectra shown in Figures 1d and 3d. Therefore, we suggest that reaction 14 does not occur under our experiment conditions.

Calculational results show that the reaction mechanism for $VO_3 + C_2H_2$ involves two processes: (1) hydrogen transfer from carbon to oxygen leading to water formation (reaction 4a); and (2) hydrogen transfer from carbon to carbon leading to ketene formation (reaction 4b). The energy barriers for these two processes are lower than the reactant energy as shown in Figure 6. Stable molecules, such as H_2O and CO_2 , are always unavoidable byproducts in the selective oxidation of hydrocarbons. The calculated results given indicate that, on a gas-phase VO_3 cluster, oxidation product (ketene) should be accompanied by a “by product” (water) formation. In a practical catalytic reaction, water formation always involves hydrogen transfer from carbon atoms to oxygen atoms, so the calculated results for reaction 4a in Figure 6 suggest mechanisms for this process. The barrier to hydrogen transfer (**14** – **14/15** – **15**) is around 1 eV if one starts with the unstable species **14** in Figure 6, for which one carbon atom forms only three bonds. The barrier (**16** – **16/17** – **17**) can be as high as ~ 2 eV if one starts from the relatively stable species (**16**). The formed H_2O molecule can adsorb on the “surface” (**17** in Figure 6) with a binding energy around 1 eV.

Note that a stable five-membered ring structure (intermediate **19**) also forms in the $VO_3 + C_2H_2$ reaction. This species is similar to intermediate **5** in the $VO_3 + C_2H_4$ reaction. The large amount of energy released in this process can be used to overcome the barriers in the later steps toward products. The $C=C$ bond of intermediate **19** is too strong to break so that $V-O$ bond cleavage leads to O atom transfer followed by dehydration and ketene production reactions. Nonetheless, in the $VO_3 + C_2H_4$ reaction, the $C-C$ single bond of intermediate **5** is relatively easy to break, and this leads to VO_2CH_2 and CH_2O products. Calculations for the $VO_3 + C_2H_2$ system are in agreement with the experimental observation that reaction 4a takes place to produce VO_2C_2 , as observed in the mass spectrum (Figures 1d and 3d). Another channel (IV) involving ketene formation through direct oxygen transfer reactions $V_mO_n + C_2H_2 \rightarrow V_mO_{n-1} + C_2H_2O$ is also thermodynamically and dynamically favorable at room temperature. If one carefully analyzes the intensity variations of neutral V_mO_n clusters in the mass spectra, then relative changes of the V_3O_6/V_3O_7 intensity ratio (Figure 1d) are found, indicating that oxygen-transfer reactions could also occur in our experiments.

7. Conclusions

The reactions of neutral vanadium oxide clusters with ethane, ethylene, and acetylene are investigated employing 26.5 eV soft X-ray laser and 10.5 eV nm laser ionizations coupled with TOF-MS for the first time. DFT calculations are applied to explore the mechanism of vanadium oxide cluster reactions with C_2 hydrocarbons. We find experimentally that reactivity for these reactions between neutral vanadium oxide clusters (V_mO_n) increases from C_2H_6 , C_2H_4 , to C_2H_2 . This reactivity is well interpreted based on the behavior of binding energies calculated for the experimental conditions. Association reactions are

identified as the major products for the $V_mO_n + C_2H_2$ reactions. Two dehydration products VO_2C_2 and VOC_4H_2 are also identified. DFT calculated results suggest that both reaction channels, dehydration (water formation) and partial oxidation (ketene formation), can occur without an overall reaction barrier for the $VO_3 + C_2H_2$ reaction. For the reaction of $V_mO_n + C_2H_4$, we observe products VO_2CH_2 , $V_3O_7CH_2$, and $V_5O_{12}CH_2$, in addition to association products. C=C bond cleavage occurs for C_2H_4 reacting with the oxygen rich neutral clusters VO_3 , V_3O_8 , and V_5O_{13} . The DFT calculations indicate that the reaction $VO_3 + C_2H_4 \rightarrow VO_2CH_2 + H_2CO$ is thermodynamically favorable and overall barrierless at room temperature. We suggest that the VO_3 moiety can be an active site for neutral vanadium oxide clusters. Another possible reaction channel, acetaldehyde formation, has about a 0.25 eV barrier although this path is thermodynamically more favorable. We conclude that neutral vanadium oxide oxygen rich clusters $VO_3-(V_2O_5)_n$, $n=0,1,2,\dots$ can break the C=C double bond of C_2H_4 to generate H_2CO . On the basis of experimental data and DFT calculations, a catalytic cycle for selective oxidation of C_2H_4

to produce formaldehyde on $VO_3/VO_3(V_2O_5)_n$, $n=0,1,2,\dots$ clusters is suggested. Understanding the catalytic characteristics of such clusters will challenge real catalyst design and synthesis. Further theoretical and experimental investigations for larger alkenes reacting with neutral vanadium oxide clusters are in progress.

Acknowledgment. This work is supported by Philip Morris, U.S.A., the U.S. DOE BES program, the NSF ERC for Extreme Ultraviolet Science and Technology under NSF Award No. 0310717, the National Center for Supercomputing Applications under Grant No. CHE070000N, the Chinese Academy of Sciences (Hundred Talents Fund), the 973 Programs (Nos. 2006CB932100 and 2006CB806200), and the National Natural Science Foundation of China (Grants Nos. 90406024, 50602007).

Supporting Information Available: DFT optimized geometries of reaction intermediates and transition states for $V_nO_m + C_2H_4/C_2H_2$. This material is available free of charge via the Internet at <http://pubs.acs.org>.

JA076007Z